

Plasmoid Motion in Helical Plasmas

Ryuichi ISHIZAKI and Noriyoshi NAKAJIMA

National Institute for Fusion Science, Toki 509-5292, Japan

(Received 12 December 2009 / Accepted 18 May 2010)

In order to explain the difference between the motion of plasmoids created by pellet injection in tokamak and helical plasmas, magnetohydrodynamic (MHD) simulations including ablation processes have been performed in tokamak and Large Helical Device (LHD) plasmas. In the LHD, plasmoid motion depends on the initial location of the plasmoid, whereas in a tokamak, the plasmoid always drifts in the direction opposite to that of the curvature vector. It is verified that there are two main forces acting on the plasmoid, and the connection length determines the dominant force.

© 2010 The Japan Society of Plasma Science and Nuclear Fusion Research

Keywords: pellet, MHD, ablation

DOI: 10.1585/pfr.5.S2060

1. Introduction

Injecting small pellets of frozen hydrogen into torus plasmas is a proven method of fueling [1]. The physical processes are divided into two stages. In the micro stage, mass is ablated at the pellet surface because it encounters high-temperature bulk plasma. The neutral gas produced by ablation is rapidly heated by electrons and ionized to form a high-density, low-temperature plasma, called a plasmoid. In the macro stage, the plasmoid is redistributed by free streaming along the magnetic field lines and by magnetohydrodynamic (MHD) processes that cause mass flow across the flux surfaces. The micro stage is well understood by an analytic method [2] and numerical simulation [3]. The drift motion of the plasmoid has been investigated in the macro stage [4]. Since the plasmoid drifts to the lower-field side, pellet fueling to make the plasmoid approach the core plasma is successful when a pellet is injected from the high-field side in a tokamak. On the other hand, such good performance has not been obtained yet in experiments in the planar axis heliotron, the Large Helical Device (LHD), even when a pellet was injected from the high-field side [5]. The purpose of this study is to explain the difference between the motion of a plasmoid in tokamak and helical plasmas. To investigate plasmoid motion, a three-dimensional (3D) MHD code including ablation processes has been developed by extending the pellet ablation code (CAP) [3, 6]. In the LHD, the drift motion depends on the initial location of the plasmoid, whereas in a tokamak, the plasmoid always drifts in the direction opposite to that of the magnetic curvature vector.

2. Plasmoid Drift Motion

Since linear theory cannot be applied to a plasmoid because of its large perturbation, a nonlinear simulation is

required to explain its behavior. Plasmoid drift motion is considered to be an MHD behavior because the drift speed obtained from experimental data [1] is several percent of v_A , where v_A is the Alfvén velocity. Thus, a 3D MHD code including ablation processes has been developed by extending the CAP [3]. In order to investigate plasmoid motion in LHD plasmas, an equilibrium obtained by the HINT code [7] is used as bulk plasma. The cubic-interpolated pseudoparticle (CIP) method is used in the code as a numerical scheme [8]. To explain the difference between plasmoid motions in a tokamak and LHD, four simulations (cases 1, 2, 3, and 4) have been performed as described in Table 1; details are shown in Figs. 1 and 2. Figure 1 (a) shows a poloidal cross section of a tokamak in case 1, in which the contours show magnetic pressure and the colors show plasma pressure. The circle represents an initial plasmoid whose peak values of density and temperature are 1000 times the density and 1/1000 times the temperature of the bulk plasma, respectively. The plasmoid, whose half-width is 0.03, encounters electrons with a fixed temperature of 2 keV and density of 10^{20} m^{-3} . The plasmoid is located inside the torus at the high-field side. The magnetic curvature vector where the plasmoid is located is negative along the major radius. Figure 1 (b) shows the plasma beta and safety factor of the tokamak. Figure 2 shows the density profiles in the direction of the major radius through

Table 1 Simulation conditions.

Case	Configuration	Plasmoid location	Poloidal cross section	Curvature vector at plasmoid
1	Tokamak	inside	—	negative
2	LHD	inside	horizontal	positive
3	LHD	outside	horizontal	negative
4	LHD	inside	vertical	negative

author's e-mail: ishizaki@nifs.ac.jp

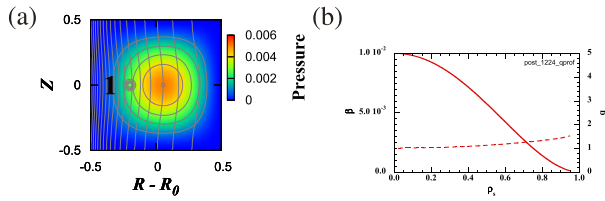


Fig. 1 (a) Poloidal cross section in case 1. Contours and colors show magnetic and plasma pressures, respectively. The circle represents an initial plasmoid. (b) Plasma beta β (solid line) and safety factor q (dashed line) as a function of normalized minor radius ρ_s .

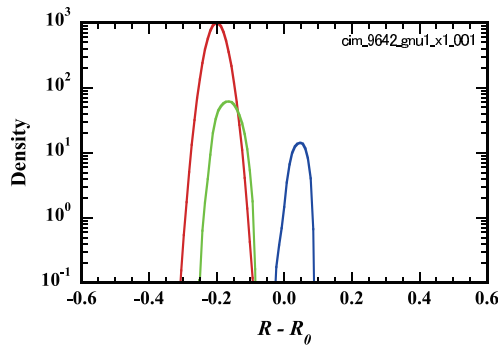


Fig. 2 Density profiles at $t = 0$ (red), 2.5 (green), and 5 (blue) in case 1.

the center of the plasmoid at $t = 0, 2.5,$ and $5,$ which is normalized by the Alfvén transit time. Since the plasmoid is rapidly elongated along the magnetic field, the density peak decreases and simultaneously drifts across the flux surface in the direction of the major radius. Thus, the plasmoid drifts in the direction opposite to that of the magnetic curvature. This motion is induced by a $1/R$ force because of the magnetic field [9]. The details are discussed in the following section.

The LHD configurations in cases 2, 3, and 4 are shown in Fig. 3. Figures 3(a) and (b) show the horizontally and vertically elongated cross sections, respectively. The contours represent magnetic pressures and the colors represent the plasma pressures. The initial plasmoids in cases 2 and 3 are shown in Fig. 3(a), and that in case 4 is shown in Fig. 3(b). The plasmoids in cases 2 and 4 are located inside the torus, and that in case 3 is located outside it. The helical plasma has a saddle point on the poloidal cross section of the magnetic pressure. Since the plasmoid in case 2 is located inside the torus and at the lower-field side compared to the saddle point, the curvature vector is positive in the major radius direction. On the other hand, since the plasmoid in case 3 is located outside the torus and at the lower-field side compared to the saddle point, the curvature vector is negative in the major radius direction. Since the plasmoid in case 4 is located inside the torus and at a higher-field side compared to the saddle point, the curvature vector is negative in the major radius direction. Figure 3(c) shows the plasma beta and rotational transform in the

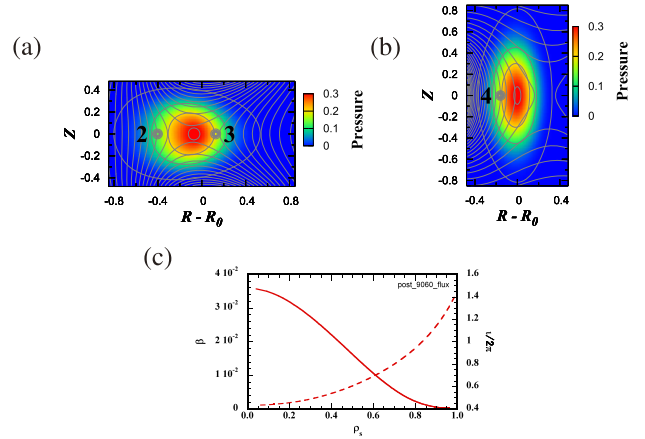


Fig. 3 Poloidal cross sections in (a) cases 2 and 3 and (b) case 4. Contours and colors show the magnetic and plasma pressures, respectively. Circles represent initial plasmoids. (c) Plasma beta β (solid line) and rotational transform $l/2\pi$ (dashed line) as a function of normalized minor radius ρ_s .

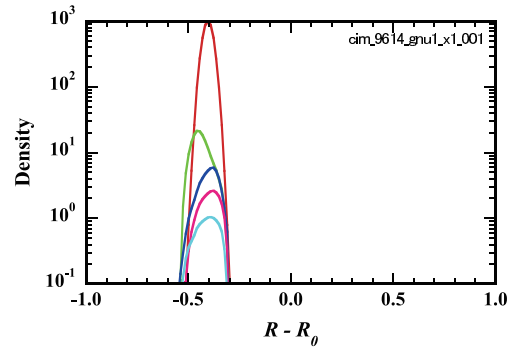


Fig. 4 Density profiles at $t = 0$ (red), 5 (green), 10 (blue), 15 (pink), and 20 (sky blue) in case 2.

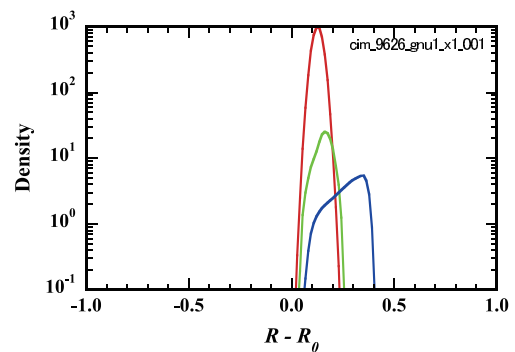


Fig. 5 Density profiles at $t = 0$ (red), 5 (green), and 10 (blue) in case 3.

LHD. The simulation results in cases 2, 3, and 4 are shown in Figs. 4, 5, and 6, respectively. In case 2, the plasmoid drifts slightly back and forth along the major radius. In case 3, it drifts in the direction of the major radius. In case 4, it drifts slightly but does not reach the magnetic axis. The results in the LHD do not correspond to those in case 1, in which the plasmoids drift in the direction opposite to

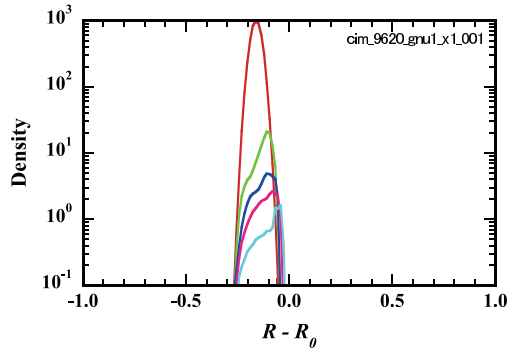


Fig. 6 Density profiles at $t = 0$ (red), 5 (green), 10 (blue), 15 (pink), and 20 (sky blue) in case 4.

that of the curvature vector. The reason is discussed in the following section.

3. Discussion

The force acting on the plasmoid is given by differentiating the MHD equilibrium as follows.

$$\begin{aligned} \mathbf{F} = & -\nabla(p_1 + \mathbf{B}_0 \cdot \mathbf{B}_1 + B_1^2/2) + \mathbf{B}_0 \cdot \nabla \mathbf{B}_1 \\ & + \mathbf{B}_1 \cdot \nabla \mathbf{B}_0 + \mathbf{B}_1 \cdot \nabla \mathbf{B}_1, \end{aligned} \quad (1)$$

where \mathbf{B}_0 is the equilibrium magnetic field, p_1 and \mathbf{B}_1 are the perturbations in the pressure and magnetic field, respectively, which are extremely large and are induced by the plasmoid. The first term represents the forces induced by the plasma pressure and magnetic pressure, which almost cancel each other because of the diamagnetic effect. The other terms represent forces dominated by the magnetic curvature. Figures 7 (a), (b), (c), and (d) show the temporal evolution of the plasmoid accelerations induced by those forces in cases 1, 2, 3, and 4, respectively. The red, green, blue, and pink lines show the accelerations due to the first, second, third, and fourth terms, respectively, in Eq. (1). The sky blue lines show the total acceleration. The second terms are leading terms in all cases. The major radius component of the second term in Eq. (1) is decomposed as follows:

$$\begin{aligned} F_R = & \mathbf{e}_R \cdot (\mathbf{B}_0 \cdot \nabla \mathbf{B}_1) \\ = & \mathbf{B}_0 \cdot \nabla B_{R1} - \frac{B_{\phi 0} B_{\phi 1}}{R}, \end{aligned} \quad (2)$$

where R is the major radius, and B_{R1} is the major radius component of the magnetic field perturbation. The first term in Eq. (2) represents the gradient of B_{R1} along the field lines, and the second term represents the $1/R$ force due to the toroidal field [9]. Figures 8 (a), (b), (c), and (d) show the temporal evolution of the plasmoid accelerations induced by those forces in cases 1, 2, 3, and 4, respectively. The red and green lines show the first and second terms, respectively, in Eq. (2). The blue lines show the accelerations due to F_R . In case 1, the second term seems to be dominant, whereas in cases 2 and 4, the first term seems to be dominant; in case 3, the dominant forces are

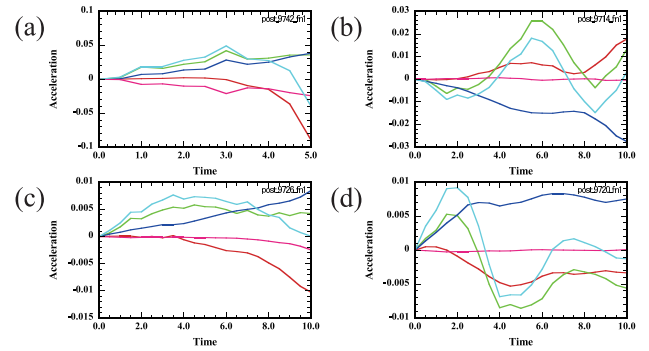


Fig. 7 Acceleration acting on the plasmoids as a function of time in cases (a) 1, (b) 2, (c) 3, and (d) 4. Red, green, blue, and pink lines show the acceleration due to the first, second, third, and fourth terms, respectively, in Eq. (1). Sky blue lines show the total acceleration.

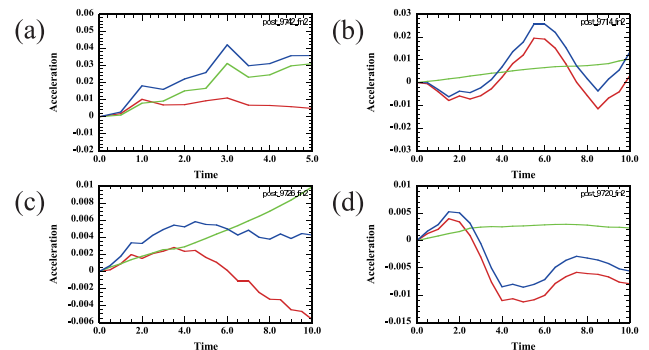


Fig. 8 Acceleration due to $\mathbf{B}_0 \cdot \nabla \mathbf{B}_1$ as a function of time in cases (a) 1, (b) 2, (c) 3, and (d) 4. Red, green, and blue lines show the acceleration due to the first, second, and total forces, respectively, in Eq. (2).

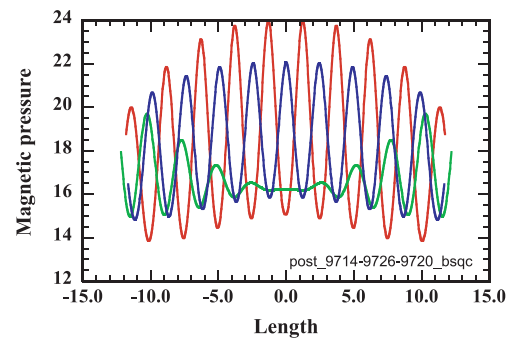


Fig. 9 Magnetic pressure B_0^2 as a function of the length along the magnetic field line ℓ . Red, green, and blue lines represent cases 2, 3, and 4 respectively.

not clear. The first term in Eq. (2) can be approximately expressed as $B_0 B_{R1}/L_c$, where L_c is the connection length depending on the configuration. In the tokamak (case 1), the connection length becomes $L_c \sim \pi q R$. The second term becomes larger than the first when $q \sim 1$. In the LHD, the connection length depends on the location of the plasmoid. Figure 9 shows the spatial profile of the equilibrium magnetic pressure along the field lines in the LHD. The red,

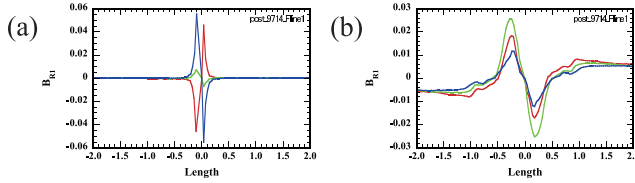


Fig. 10 B_{R1} as a function of the length along the magnetic field lines ℓ in case 2 at (a) $t = 0.5$ and (b) $t = 2.5$. Red, green, and blue lines are different field lines through the plasmoid.

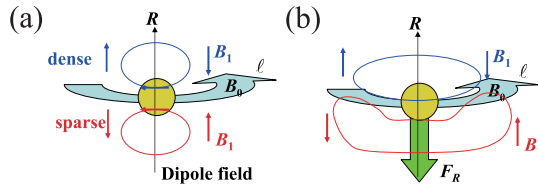


Fig. 11 Magnetic field around the plasmoid in case 2 at (a) $t = 0.5$ and (b) $t = 2.5$.

green, and blue lines correspond to the magnetic field lines through the plasmoid in cases 2, 3, and 4, respectively, where the plasmoids are located at $\ell = 0$. The connection length in case 3 becomes longer than those in cases 2 and 4 because the deviation of the magnetic pressure around the plasmoid is small in case 3. This difference due to the locations is defined by $\alpha (\leq 1)$; the connection length in the LHD is expressed as $L_c = \pi R / \alpha M$, where $\alpha = 1$ in cases 2 and 4 and $\alpha < 1$ in case 3, and M is the toroidal pitch number. By using $M = 10$, $\alpha = 1$, and $R = 3.82$, which is the major radius at the center of the poloidal cross section, the connection length becomes ~ 1.2 , which corresponds to the red and blue lines in Fig. 9. Since the first term in Eq. (2) is given by $\alpha M B_0 B_{R1} / \pi R$ in the LHD, it becomes the leading one because $\alpha = 1$ in cases 2 and 4. On the other hand, both terms become dominant because $\alpha < 1$ in case 3. Those evaluations correspond to the results in Figs. 8 (b), (c), and (d), respectively.

The first term in Eq. (2) clearly has oscillations, as shown in Figs. 8 (b) and (d). The plasmoid motions in Figs. 4 and 6 are induced by such oscillations. The oscillations can be explained as follows: Figure 10 shows the spatial profiles of B_{R1} along the field lines in case 2. The magnetic field lines denoted by red, green, and blue pass through different cylindrical coordinates of the plasmoid, i.e., $(R_0 - \Delta, 0, 0)$, $(R_0, 0, 0)$, and $(R_0 + \Delta, 0, 0)$, respectively, where $(R_0, 0, 0)$ is the center of the plasmoid and Δ is extremely small. Figures 11 (a) and (b) show physical images explaining Figs. 10 (a) and (b), respectively. The perturbed magnetic field around the plasmoid is transformed into a dipole field because of the diamagnetic effect, as shown in Fig. 11 (a). Since the curvature vector of the equilibrium magnetic field is positive in the major radius direction, the field lines become dense and sparse in the upper (blue) and lower (red) regions of the field lines, respectively, through

the center of the plasmoid (Fig. 11 (a)). Thus, the magnitude of the upper field line is larger than that of the lower one. Those physical images correspond to Fig. 10 (a), in which the red and blue lines have opposite phases and the maximum absolute value of the blue line is larger than that of the red line. Subsequently, deformation of the dipole fields is induced by the difference between the strengths of the upper and lower field lines, as shown in Fig. 11 (b). Therefore, all the lines in Fig. 10 (b) have the same phase as the blue line in Fig. 10 (a). Since the term $\partial B_{R1} / \partial \ell$ becomes negative on all the lines, the force acting on the plasmoid becomes negative in the major radius direction according to Eq. (2). On the other hand, the magnetic field has a restoring force due to the tension. Then, the oscillation of the field lines is driven by the restoring force, which dominates the total acceleration in Fig. 7 (b). Since the negative acceleration ($0 < t < 4$) is slightly smaller than the positive acceleration ($4 < t < 7.5$), as shown in Fig. 7 (b), the plasmoid drifts back and forth, as shown in Fig. 4. In case 4, the first term shows oscillation because of the same physics, but it continues to be negative at $t > 2$, as shown in Fig. 8 (d). However, since the acceleration is added by the other force, the total acceleration oscillates around zero, as shown in Fig. 7 (d). As a result, the plasmoid drifts slightly because the positive acceleration ($0 < t < 3.5$) is slightly larger than the negative acceleration ($3.5 < t < 6.5$), as shown in Fig. 7 (d). Although the plasmoid motion is quantitatively determined by the sum of all the forces, in cases 2 and 4, it is mainly determined by the first term in Eq. (2). In case 3, the first and second terms become comparable because the connection length is long, as shown in Fig. 9. Since the second term in Eq. (2) is always positive because of the diamagnetic effect, the plasmoid has a positive acceleration, as shown in Fig. 7 (c).

4. Summary

It is verified by simulations using the CAP code that the motions of plasmoids with a high pressure induced by heat flux are different between a tokamak and the LHD. The plasmoid drifts in the direction opposite to the magnetic curvature vector in a tokamak. In contrast, in the LHD, the plasmoid drifts slightly back and forth along the major radius when it is initially located inside the torus on the horizontally elongated cross section. It drifts slightly in the major radius direction, but does not reach the magnetic axis when it is initially located inside the vertically elongated cross section. It drifts in the major radius direction when it is initially located outside the horizontally elongated cross section. The plasmoid motion is determined mainly by the $1/R$ force due to the toroidal field and the force due to the gradient of B_{R1} along the field line. The former force implies a drift in the direction opposite to the curvature vector, which is dominant in a tokamak. Since the latter forces are dominant when the plasmoids are lo-

cated inside the torus in the LHD, the plasmoid motions in the LHD differ from those in a tokamak. It is verified that the connection length determines the force that dominates the plasmoid motion. This may explain the difference in the behavior of the plasmoid motion in tokamaks and the LHD.

- [1] Y. W. Muller *et al.*, Nucl. Fusion **42**, 301 (2002).
- [2] P. B. Parks and M. N. Rosenbluth, Phys. Plasmas **5**, 1380 (1998).
- [3] R. Ishizaki *et al.*, Phys. Plasmas **11**, 4064 (2004).
- [4] P. B. Parks *et al.*, Phys. Rev. Lett. **94**, 125002 (2005).
- [5] R. Sakamoto *et al.*, in *proceedings of 29th EPS conference on Plasma Phys. and Control. Fusion*.
- [6] R. Ishizaki *et al.*, IAEA-CN-149/TH/P3-6 (2006).
- [7] K. Harafuji *et al.*, J. Comput. Phys. **81**, 169 (1989).
- [8] H. Takewaki *et al.*, J. Comput. Phys. **61**, 261 (1985).
- [9] J. P. Freidberg, *Ideal Magnetohydrodynamics* (Plenum Press, New York, 1987).